A proximal iteration for deconvolving Poisson noisy images using sparse representations

François-Xavier Dupé, Jalal M. Fadili, Jean-Luc Starck

A proximal iteration for deconvolving Poisson noisy images using sparse representations

F.-X. Dupé[a], M.J. Fadili[a] and J.-L. Starck[b]

[a] GREYC UMR CNRS 6072 [b] DAPNIA/SEDI-SAP CEA-Saclay

14050 Caen France 91191 Gif-sur-Yvette France

Abstract

We propose an image deconvolution algorithm when the data is contaminated by Poisson noise. The image to restore is assumed to be sparsely represented in a dictionary of waveforms such as the wavelet or curvelet transforms. Our key contributions are: First, we handle the Poisson noise properly by using the Anscombe variance stabilizing transform leading to a *non-linear* degradation equation with additive Gaussian noise. Second, the deconvolution problem is formulated as the minimization of a convex functional with a data-fidelity term reflecting the noise properties, and a non-smooth sparsity-promoting penalties over the image representation coefficients (e.g. ℓ_1-norm). Third, a fast iterative backward-forward splitting algorithm is proposed to solve the minimization problem. We derive existence and uniqueness conditions of the solution, and establish convergence of the iterative algorithm. Finally, a GCV-based model selection procedure is proposed to objectively select the regularization parameter. Experimental results are carried out to show the striking benefits gained from taking into account the Poisson statistics of the noise. These results also suggest that using sparse-domain regularization may be tractable in many deconvolution applications with Poisson noise such as astronomy and microscopy.

Index Terms

Deconvolution, Poisson noise, Proximal iteration, forward-backward splitting, Iterative thresholding, Sparse representations.

I. Introduction

Deconvolution is a longstanding problem in many areas of signal and image processing (e.g. biomedical imaging [1], [2], astronomy [3], remote-sensing, to quote a few). For example, research in astronomical image deconvolution has recently seen considerable work, partly triggered by the Hubble space telescope (HST) optical aberration problem at the beginning of its mission. In biomedical imaging, researchers are also increasingly relying on deconvolution to improve the quality of images acquired by confocal microscopes [2]. Deconvolution may then prove crucial for exploiting images and extracting scientific content.

There is an extensive literature on deconvolution problems. One might refer to well-known dedicated monographs on the subject [4]–[6]. In presence of Poisson noise, several deconvolution methods have been proposed such as Tikhonov-Miller inverse filter and Richardson-Lucy (RL) algorithms; see [1], [3] for a comprehensive review. The RL has been used extensively in many applications because it is adapted to Poisson noise. The RL algorithm, however, amplifies noise after a few iterations, which can be avoided by introducing regularization. In [7], the authors presented a Total Variation (TV)-regularized RL algorithm. In the astronomical imaging literature, several authors advocated the use of wavelet-regularized RL algorithm [8]–[10]. In the context of biological imaging deconvolution, wavelets have also been used as a regularization scheme when deconvolving biomedical images; [11] presents a version of RL combined with wavelets denoising, and [12] uses the thresholded Landweber iteration introduced in [13]. The latter approach implicitly assumes that the contaminating noise is Gaussian.

In the context of deconvolution with Gaussian white noise, sparsity-promoting regularization over orthogonal wavelet coefficients has been recently proposed [13]–[15]. Generalization to frames was proposed in [16], [17]. In [18], the authors presented an image deconvolution algorithm by iterative thresholding in an overcomplete dictionary of transforms, and [19] designed a deconvolution method that combines both the wavelet and curvelet transforms. However, all sparsity-based approaches published so far have mainly focused on Gaussian noise.

In this paper, we propose an image deconvolution algorithm for data blurred and contaminated by Poisson noise. The Poisson noise is handled properly by using the Anscombe variance stabilizing transform (VST), leading to a *non-linear* degradation equation with additive Gaussian noise, see (1). The deconvolution problem is then formulated as the minimization of a convex functional with a non-linear data-fidelity term reflecting the noise properties, and a non-smooth sparsity-promoting penalty over the representation coefficients of the image to restore, e.g. wavelet or curvelet coefficients. Inspired by the work in [15], a fast proximal iterative algorithm is proposed to solve the minimization problem. Experimental results are carried out on a set of simulated and real images to compare our approach to some competitors. We show the striking benefits gained from taking into account the Poisson nature of the noise and the morphological structures involved in the image through overcomplete sparse multiscale transforms.

A. Relation to prior work

A naive solution to this deconvolution problem would be to apply traditional approaches designed for Gaussian noise. But this would be awkward as (i) the noise tends to Gaussian only for large mean intensities (central limit

theorem), and (ii) the noise variance depends on the mean anyway. A more adapted way would be to adopt a bayesian framework with an adapted anti-log-likelihood score (i.e. data fidelity term) reflecting the Poisson statistics of the noise. Unfortunately, doing so, we would end-up with a functional which does not satisfy a key property: the data fidelity term does not have a Lipschitz-continuous gradient as required in [15], hence preventing us from using the forward-backward splitting proximal algorithm to solve the optimization problem. To circumvent this difficulty, we propose to handle the noise statistical properties by using the Anscombe VST. Some previous authors [20] have already suggested to use the Anscombe VST, and then deconvolve with wavelet-domain regularization as if the stabilized observation were linearly degraded and contaminated by additive Gaussian noise. But this is not valid as standard asymptotic results of the Anscombe VST is not-linear because of the square-root, see (1).

B. Organization of this paper

The organization of the paper is as follows: we first formulate our deconvolution problem under Poisson noise (Section II), and then recall some necessary material about overcomplete sparse representations (Section III). The core of the paper lies in Section IV, where we state the deconvolution optimization problem, characterize it and solve it using monotone operator splitting iterations. We also focus on the choice of the two main parameters of the algorithm and propose some solutions. In Section V, experimental results are reported and discussed. The proofs of our main results are deferred to the appendix awaiting inspection by the interested reader.

C. Notation

Let $\mathcal{H}$ a real Hilbert space, here a finite dimensional vector subspace of $\mathbb{R}^n$. We denote by $\|.\|$ the norm associated with the inner product $\langle .,. \rangle$ in $\mathcal{H}$, and I is the identity operator on $\mathcal{H}$. x and α are respectively reordered vectors of image samples and transform coefficients. A function f is coercive, if $\lim_{\|x\| \to +\infty} f(x) = +\infty$. The domain of f is defined by $\operatorname{dom} f = \{x \in \mathcal{H} \ : \ f(x) < +\infty\}$ and f is proper if $\operatorname{dom} f \neq \emptyset$. An operator A acting on $\mathcal{H}$ is κ-Lipschitz continuous if $\forall x, y \in \mathcal{H}, \|\mathrm{A}(x) - \mathrm{A}(y)\| \leqslant \kappa \|x - y\|$ where κ is the Lipschitz constant. $\Gamma_0(\mathcal{H})$ is the class of all proper lower semi-continuous (lsc) convex functions from $\mathcal{H}$ to $]-\infty, +\infty]$. We denote by $\imath_{\mathcal{C}}$ the indicator of the convex set $\mathcal{C}$: $\imath_{\mathcal{C}}(x) = \begin{cases} 0, & \text{if } x \in \mathcal{C} \ , \\ +\infty, & \text{otherwise.} \end{cases}$. We denote by $\rightharpoonup$ the weak convergence (from weak topology to weak topology).

II. Problem statement

Consider the image formation model where an input image of n pixels x is blurred by a point spread function (PSF) h and contaminated by Poisson noise. The observed image is then a discrete collection of counts $y = (y_i)_{1 \leqslant i \leqslant n}$ which are bounded, i.e. $y \in \ell_\infty$. Each count y_i is a realization of an independent Poisson random variable with a mean $(h \circledast x)_i$, where $\circledast$ is the circular convolution operator. Formally, this writes $y_i \sim \mathcal{P}((h \circledast x)_i)$. The deconvolution problem at hand is to restore x from the observed count image y.

A natural way to attack this problem would be to adopt a maximum a posteriori (MAP) bayesian framework with an appropriate anti-log-likelihood score (i.e. data fidelity term) reflecting the Poisson statistics of the noise. But, as stated above, this would prevent us from using the backward-forward splitting proximal algorithm to solve the MAP optimization problem, since the gradient of the data fidelity term is not Lipschitz-continuous. We then propose to handle the noise statistical properties by using the Anscombe VST [21] defined as

$$z_i = 2\sqrt{(h \circledast x)_i + \tfrac{3}{8}} + \varepsilon, \quad \varepsilon \sim \mathcal{N}(0,1), \tag{1}$$

where ε is an additive white Gaussian noise of unit variance[1]. In words, z is *non-linearly* related to x. In Section IV, we provide an elegant optimization problem and a fixed point algorithm taking into account such a non-linearity.

III. Sparse image representation

Let $x \in \mathcal{H}$ be an $\sqrt{n} \times \sqrt{n}$ image. x can be written as the superposition of elementary atoms φ_γ parameterized by $\gamma \in \mathcal{I}$ according to the following generative model :

$$x = \sum_{\gamma \in \mathcal{I}} \alpha_\gamma \varphi_\gamma = \Phi\alpha, \quad |\mathcal{I}| = L \geqslant n \ . \tag{2}$$

We denote by Φ the dictionary i.e. the $n \times L$ matrix whose columns are the generating waveforms $(\varphi_\gamma)_{\gamma \in \mathcal{I}}$ all normalized to a unit ℓ_2-norm. The forward (analysis) transform is then defined by a non-necessarily square matrix $\mathbf{T} = \Phi^{\mathrm{T}} \in \mathbb{R}^{L \times n}$ with $L \geqslant n$. When $L > n$ the dictionary is said to be redundant or overcomplete. In the case of the simple orthogonal basis, the inverse (synthesis) transform is trivially $\Phi = \mathbf{T}^{\mathrm{T}}$. Whereas assuming that Φ is a tight frame implies that the frame operator satisfies $\Phi\Phi^{\mathrm{T}} = c\mathrm{I}$, where $c > 0$ is the tight frame constant. For tight frames, the pseudo-inverse reconstruction (synthesis) operator reduces to $c^{-1}\Phi$. In the sequel, the dictionary Φ will correspond to an orthobasis or a tight frame of $\mathcal{H}$.

Owing to recent advances in modern harmonic analysis, many redundant systems, like the undecimated wavelet transform, curvelet, contourlet, were shown to be very effective in sparsely representing images. By sparsity, we mean that we are seeking for a good representation of x with only few significant coefficients.

In the rest of the paper, the dictionary Φ is built by taking union of one or several (sufficiently incoherent) transforms, each corresponding to an orthogonal basis or a tight frame. Choosing an appropriate dictionary is a key step towards a good sparse representation, hence restoration. A core idea here is the concept of morphological diversity. When the transforms are amalgamated in the dictionary, they have to be chosen such that each leads to sparse representations over the parts of the images it is serving, e.g. wavelets for smooth images with isotropic singularities [22], curvelets for representing piecewise smooth C^2 images away from C^2 contours [23], [24], wave atoms of local DCT to represent warped locally oscillating textures [22], [25].

[1]Rigorously speaking, the equation is to be understood in an asymptotic sense.

IV. Sparse Iterative Deconvolution

A. Optimization problem

The class of minimization problems we are interested in can be stated in the general form :

$$\min_{x\in\mathcal{H}} f_1(x) + f_2(x), \tag{3}$$

where $f_1 \in \Gamma_0(\mathcal{H})$, $f_2 \in \Gamma_0(\mathcal{H})$ and f_1 is differentiable with a κ-Lipschitz gradient. We denote by $\mathcal{M}$ the set of solutions of (3).

From (1), we immediately deduce the data fidelity term

$$F \circ \mathrm{H} \circ \Phi\ (\alpha), \text{ with} \tag{4}$$
$$F : \eta \in \mathbb{R}^n \mapsto \sum_{i=1}^{n} f(\eta_i), \quad f(\eta_i) = \frac{1}{2}\left(z_i - 2\sqrt{\eta_i + \tfrac{3}{8}}\right)^2,$$

where H denotes the (block-Toeplitz) convolution operator. From a statistical perspective, (4) corresponds to the anti-log-likelihood score.

Adopting a bayesian framework and using a standard MAP rule, our goal is to minimize the following functional with respect to the representation coefficients α :

$$(\mathsf{P}_{\lambda,\psi}) : \min_{\alpha} J(\alpha)\ , \tag{5}$$
$$J : \alpha \mapsto \underbrace{F \circ \mathrm{H} \circ \Phi\ (\alpha)}_{f_1(\alpha)} + \underbrace{\imath_{\mathcal{C}} \circ \Phi\ (\alpha) + \lambda \sum_{i=1}^{L} \psi(\alpha_i)}_{f_2(\alpha)},$$

where we implicitly assumed that $(\alpha_i)_{1\leqslant i\leqslant L}$ are independent and identically distributed with a Gibbsian density $\propto e^{-\lambda\psi(\alpha_i)}$. The penalty function ψ is chosen to enforce sparsity, $\lambda > 0$ is a regularization parameter and $\imath_{\mathcal{C}}$ is the indicator function of the convex set $\mathcal{C}$. In our case, $\mathcal{C}$ is the positive orthant. We remind that the positivity constraint is because we are fitting Poisson intensities, which are positive by nature. We also define the set $\mathcal{C}' = \{\alpha | \Phi\alpha \in \mathcal{C}\}$, that is $\imath_{\mathcal{C}'} = \imath_{\mathcal{C}} \circ \Phi$.

From (5), we have the following,

Proposition 1.

(i) *f_1 is convex function. It is strictly convex if Φ is an orthobasis and $\ker(\mathrm{H}) = \emptyset$ (i.e. the spectrum of the PSF does not vanish within the Nyquist band).*

(ii) *The gradient of f_1 is*

$$\nabla f_1(\alpha) = \Phi^{\mathrm{T}} \circ \mathrm{H}^* \circ \nabla F \circ \mathrm{H} \circ \Phi\ (\alpha)\ , \tag{6}$$

with

$$\nabla F(\eta) = \left(\frac{-z_i}{\sqrt{\eta_i + 3/8}} + 2\right)_{1\leqslant i\leqslant n}. \tag{7}$$

(iii) f_1 *is continuously differentiable with a* κ*-Lipschitz gradient where*

$$\kappa \leqslant \left(\tfrac{2}{3}\right)^{3/2} 4c \left\|\mathrm{H}\right\|_2^2 \left\|z\right\|_\infty < +\infty. \tag{8}$$

(iv) $(\mathsf{P}_{\lambda,\psi})$ *is a particular case of problem* (3)*.*

A proof can be found in the appendix.

B. Characterization of the solution

Since J is coercive and convex, the following holds:

Proposition 2.

1) *Existence:* $(\mathsf{P}_{\lambda,\psi})$ *has at least one solution, i.e.* $\mathcal{M} \neq \emptyset$*.*
2) *Uniqueness:* $(\mathsf{P}_{\lambda,\psi})$ *has a unique solution if* Φ *is an orthobasis and* $\ker(\mathrm{H}) = \emptyset$*, or if* ψ *is strictly convex.*

C. Proximal iteration

We first define the notion of a proximity operator, which was introduced in [26] as a generalization of the notion of a convex projection operator.

Definition 1 (Moreau [26]). *Let* $\varphi \in \Gamma_0(\mathcal{H})$*. Then, for every* $x \in \mathcal{H}$*, the function* $y \mapsto \varphi(y) + \|x-y\|^2/2$ *achieves its infimum at a unique point denoted by* $\mathrm{prox}_\varphi\, x$*. The operator* $\mathrm{prox}_\varphi : \mathcal{H} \to \mathcal{H}$ *thus defined is the proximity operator of* φ*. Moreover,* $\forall x, p \in \mathcal{H}$

$$\begin{aligned} p = \mathrm{prox}_\varphi\, x \iff & x - p \in \partial\varphi(p) \\ \iff & \langle y - p, x - p\rangle + \varphi(p) \leqslant \varphi(y)\ \forall y \in \mathcal{H}. \end{aligned} \tag{9}$$

(9) *means that* prox_φ *is the resolvent of the subdifferential of* φ *[27].*

It will also be convenient to introduce the reflection operator $\mathrm{rprox}_\varphi = 2\,\mathrm{prox}_\varphi - \mathrm{I}$.

For notational simplicity, we denote by Ψ the function $\alpha \mapsto \sum_i \psi(\alpha_i)$. Our goal now is to express the proximity operator associated to f_2, which will be needed in the iterative deconvolution algorithm. The difficulty stems from the definition of f_2 which combines both the constraint and the regularization. Unfortunately, we can show that even with a separable penalty $\Psi(\alpha)$, the operator $\mathrm{prox}_{f_2} = \mathrm{prox}_{\imath_{\mathcal{C}} \circ \Phi + \lambda\Psi}$ has no explicit form in general, except the case where $\Phi = \mathrm{I}$. We then propose to replace explicit evaluation of prox_{f_2} by a sequence of calculations that activate separately $\mathrm{prox}_{\imath_{\mathcal{C}} \circ \Phi}$ and $\mathrm{prox}_{\lambda\Psi}$. We will show that the last two proximity operators have closed-form expressions. Such a strategy is known as a splitting method of monotone operators [27], [28]. As both $\imath_{\mathcal{C}'}$ and $\Psi \in \Gamma_0(\mathcal{H})$ but non-differentiable, our splitting method is based on the Douglas-Rachford algorithm [27], [29]. The following lemma summarizes our scheme.

Lemma 1. *Let Φ an orthobasis or a tight frame with constant c.*

1) If $\alpha \in \mathcal{C}'$ then $\operatorname{prox}_{f_2}(\alpha) = \operatorname{prox}_{\lambda\Psi}(\alpha)$.

2) Otherwise, let $\sum_t \nu_t(1-\nu_t) = +\infty$. Take $\gamma^0 \in \mathcal{H}$, and define the sequence of iterates:

$$\gamma^{t+1} = \gamma^t + \nu_t \left(\operatorname{rprox}_{\lambda\Psi + \frac{1}{2}\|\cdot-\alpha\|^2} \circ \operatorname{rprox}_{\imath_{\mathcal{C}'}} - \mathrm{I} \right)(\gamma^t), \tag{10}$$

where $\operatorname{prox}_{\lambda\Psi+\frac{1}{2}\|\cdot-\alpha\|^2}(\gamma^t) = \left(\operatorname{prox}_{\frac{\lambda}{2}\psi}(\alpha_i + \gamma_i^t) \right)_{1\leqslant i\leqslant L}$, $\mathcal{P}_{\mathcal{C}'} = \operatorname{prox}_{\imath_{\mathcal{C}'}} = c^{-1}\Phi^{\mathrm{T}} \circ \mathcal{P}_{\mathcal{C}} \circ \Phi + \left(\mathrm{I} - c^{-1}\Phi^{\mathrm{T}} \circ \Phi\right)$ and $\mathcal{P}_{\mathcal{C}}$ is the projector onto the positive orthant $(\mathcal{P}_{\mathcal{C}}\eta)_i = \max(\eta_i, 0)$. Then,

$$\gamma^t \rightharpoonup \gamma \text{ and } \operatorname{prox}_{f_2}(\alpha) = \mathcal{P}_{\mathcal{C}'}(\gamma). \tag{11}$$

The proof is detailed in the appendix. Note that when Φ is an orthobasis, $\mathcal{P}_{\mathcal{C}'} = \Phi^{\mathrm{T}} \circ \mathcal{P}_{\mathcal{C}} \circ \Phi$.

To implement the above iteration, we need to express $\operatorname{prox}_{\lambda\psi}$, which is given by the following result for a wide class of penalties ψ:

Lemma 2. *Suppose that ψ satisfies, (i) ψ is convex even-symmetric , non-negative and non-decreasing on $[0, +\infty)$, and $\psi(0) = 0$. (ii) ψ is twice differentiable on $\mathbb{R} \setminus \{0\}$. (iii) ψ is continuous on $\mathbb{R}$, it is not necessarily smooth at zero and admits a positive right derivative at zero $\psi'_+(0) = \lim_{h\to 0^+} \frac{\psi(h)}{h} > 0$. Then, the proximity operator $\operatorname{prox}_{\delta\psi}(\gamma) = \bar{\alpha}(\gamma)$ has exactly one continuous solution decoupled in each coordinate γ_i :*

$$\bar{\alpha}_i(\gamma_i) = \begin{cases} 0 & \text{if } |\gamma_i| \leqslant \delta\psi'_+(0) \\ \gamma_i - \delta\psi'(\bar{\alpha}_i) & \text{if } |\gamma_i| > \delta\psi'_+(0) \end{cases} \tag{12}$$

A proof of this lemma can be found in [30]. A similar result also has recently appeared in [31]. Among the most popular penalty functions ψ satisfying the above requirements, we have $\psi(\alpha_i) = |\alpha_i|$, in which case the associated proximity operator is the celebrated soft-thresholding.

We are now ready to state our main proximal iterative algorithm to solve the minimization problem $(\mathsf{P}_{\lambda,\psi})$:

Theorem 1. *For $t \geq 0$, let $(\mu_t)_t$ be a sequence in $]0, +\infty[$ such that $0 < \inf_t \mu_t \leqslant \sup_t \mu_t < \left(\frac{3}{2}\right)^{3/2} / \left(2c\,\|\mathrm{H}\|_2^2\,\|z\|_\infty\right)$, let $(\beta_t)_t$ be a sequence in $]0, 1]$ such that $\inf_t \beta_t > 0$, and let $(a_t)_t$ and $(b_t)_t$ be sequences in $\mathcal{H}$ such that $\sum_t \|a_t\| < +\infty$ and $\sum_t \|b_t\| < +\infty$. Fix $\alpha^0 \in \mathcal{H}$, for every $t \geqslant 0$, set*

$$\alpha^{t+1} = \alpha^t + \beta_t(\operatorname{prox}_{\mu_t f_2}\left(\alpha^t - \mu_t\left(\nabla f_1(\alpha^t) + b_t\right)\right) + a_t - \alpha^t) \tag{13}$$

where ∇f_1 and $\operatorname{prox}_{\mu_t f_2}$ are given by Proposition 1(ii) and Lemma 1. Then $(\alpha_t)_{t\geq 0}$ converges (weakly) to a solution of $(\mathsf{P}_{\lambda,\psi})$.

This is the most general convergence result known on the forward-backward iteration. The role of the sequences a_t and b_t is to prove the robustness of the algorithm to errors when computing the gradient ∇f_1 and the proximity operator $\operatorname{prox}_{f_2}$. The latter remark will allow us to accelerate the algorithm when Φ is a tight frame, by running the sub-iteration (10) only few iterations (and even only one iteration, see implementation details in IV-F).

D. Choice of μ

The relaxation parameter μ has an important impact on the convergence speed of the algorithm. The upper-bound provided by Theorem 1, which is derived from the Lipschitz constant (8), may be pessimistic in some applications. To circumvent this drawback, Tseng proposed in [32] an extension of the forward-backward algorithm with an iteration to adaptively estimate a "good" value of μ. The main result provided hereafter is an adaptation to our context to the one of Tseng [32]. We state it in full for the sake of completeness and the reader convenience.

Theorem 2. *Let $\mathcal{C}'$ as defined above (IV-A). Choose any $\alpha_0 \in \mathcal{C}'$. Let $(\mu_t)_{t\in\mathbb{N}}$ be a sequence such that $\forall t > 0, \mu_t \in (0,\infty)$. Let f_1 as defined in* (5)*. Then the sequence $(\alpha_t)_{t\in\mathbb{N}}$ of iterates*

$$\begin{aligned} \alpha_{t+\frac{1}{2}} &= \operatorname{prox}_{\lambda\Psi}\left(\alpha_t - \mu_t \nabla f_1(\alpha_t)\right) \ , \\ \alpha_{t+1} &= \mathcal{P}_{\mathcal{C}'}\left(\alpha_{t+\frac{1}{2}} - \mu_t\left(\nabla f_1(\alpha_{t+\frac{1}{2}}) - \nabla f_1(\alpha_t)\right)\right) \end{aligned} \tag{14}$$

converges weakly to a minimum of J.

As ∇f_1 is Lipschitz-continuous, choosing μ_t is rather easy. Indeed, using an Armijo-Goldstein-type stepsize approach, we can compute and update μ_t at each iteration by taking μ_t to be the largest $\mu \in \{\sigma, \eta\sigma, \eta^2\sigma, \ldots\}$ satisfying

$$\mu \left\| \nabla f_1(\alpha_{t+\frac{1}{2}}) - \nabla f_1(\alpha_t) \right\| \leqslant \theta \left\| \alpha_{t+\frac{1}{2}} - \alpha_t \right\| \ , \tag{15}$$

where $\eta \in (0,1)$, $\theta \in (0,1)$ and $\sigma > 0$ are constants.

It is worth noting that for tight frames, this algorithm will somewhat simplify the computation of $\operatorname{prox}_{f_2}$, removing the need of the Douglas-Rachford sub-iteration (10). But, whatever the transform, this will come at the price of keeping track of the gradient of f_2 at the points $\alpha_{t+\frac{1}{2}}$ and α_t, and the need to check (15) several times.

E. Choice of λ

As usual in regularized inverse problems, the choice of λ is crucial as it represents the desired balance between sparsity (regularization) and deconvolution (data fidelity). For a given application and corpus of images (e.g. confocal microscopy), a naive brute-force approach would consist in testing several values of λ and taking the best one by visual assessment of the deconvolution quality. However, this is cumbersome in the general case.

We propose to objectively select the regularizing parameter λ based on the generalized cross validation (GCV) [33]. GCV attempts to provide a data-driven estimate of λ by minimizing :

$$\mathrm{GCV}(\lambda) = \frac{\left\| z - 2\sqrt{\mathrm{H}\Phi\alpha^* + \frac{3}{8}} \right\|^2}{df^2}, \tag{16}$$

where α^* denotes the solution arrived at either by iteration (13) or (14), and df is the effective number of degrees of freedom.

Deriving the exact analytical form of df is very challenging in our case as it faces two main difficulties, (i) the observation model (1) is non-linear, and (ii) the solution α^* is not known in closed form but given by the forward-backward algorithm (13). Nonetheless, in the case of ℓ_1-penalty[2], and using a series of simplifying assumptions, an approximate closed-form expression of df is shown in the appendix. It is given by

$$df \approx \sum_{i=1}^{n} \frac{\lambda}{\lambda + \frac{8c}{3} \|\alpha^*\|_\infty |\hat{h}_i|^2} , \tag{17}$$

where c is again the tight frame constant and $\hat{h}$ is the discrete Fourier transform of the PSF h.

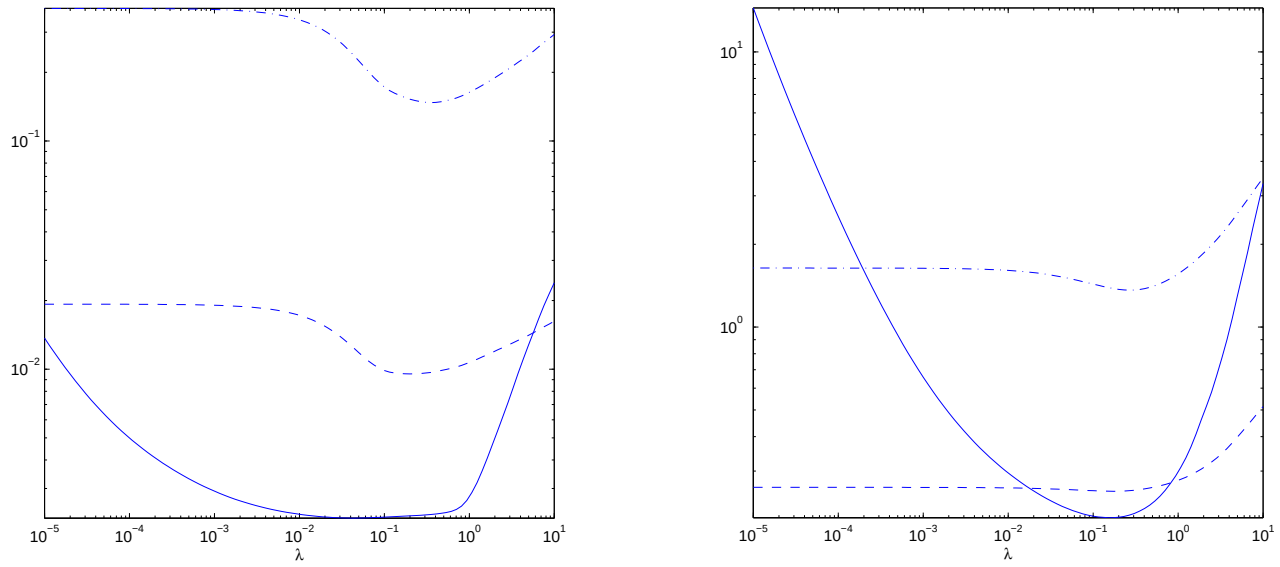

(a) (b)

Figure 1. GCV for the cameraman(a) and the neuron phantom(b) using the wavelet orthogonal transform (the solid line represents the GCV, the dashed-line the MSE and the dashed-dotted line the MAE)

Although this formula is only an approximation and its proof requires simplifying assumptions, in all our experiments, it performed very well. This is testified by Fig. 1(a) and (b) which respectively show the behavior of the GCV as a function of λ for two images: the Cameraman portrayed in Fig. 4(a) and the neuron phantom shown in Fig. 2(a). As the ground-truth is known in the simulation, we also give for each λ the mean absolute-error (MAE adapted to Poisson noise) and the mean square-error (MSE) between the deconvolved and true image. We can clearly see that the GCV reaches its minimum very close to those of the MAE and the MSE.

F. Computational complexity and implementation details

The bulk of computation of our deconvolution algorithm is invested in applying Φ (resp. H) and its adjoint Φ^{T} (resp. H^*). These operators are never constructed explicitly, rather they are implemented as fast implicit operators taking a vector x, and returning Φx (resp. $\Phi^{\mathrm{T}} x$) and $\mathrm{H}x$ (resp. $\mathrm{H}^* x$). Multiplication by H or H^* costs two FFTs, that

[2]In fact, similar derivations can be carried out for any convex ℓ_p penalty.

is $2n \log n$ operations (n denotes the number of pixels). The complexity of Φ and Φ^{T} depends on the transforms in the dictionary: for example, the wavelet orthogonal transform costs $\mathcal{O}(n)$ operations, the curvelet transform costs $\mathcal{O}(n \log n)$, etc. Let V_Φ denote the complexity of applying the analysis or synthesis operator. Define N_{FB} and N_{DR} as the number of iterations in the forward-backward algorithm and the Douglas-Rachford sub-iteration, and recall that L is the number of coefficients. The computational complexities of our iterations (13) and (14) are summarized below:

Algorithm	Computational complexity bounds	
	Φ orthobasis	Φ tight frame
(13)	$N_{\mathrm{FB}}\left(4n \log n + N_{\mathrm{DR}}\left(2V_\Phi + \mathcal{O}(n)\right)\right)$	$N_{\mathrm{FB}}\left(4n \log n + 2V_\Phi + N_{\mathrm{DR}}(2V_\Phi + \mathcal{O}(L))\right)$
(14)	$N_{\mathrm{FB}}\left(8n \log n + 2V_\Phi + \mathcal{O}(n)\right)$	$N_{\mathrm{FB}}\left(8n \log n + 6V_\Phi + \mathcal{O}(L)\right)$

The orthobasis case requires less multiplications by Φ and Φ^{T} because in that case, Φ is a bijective linear operator. Thus, the optimization problem (5) can be equivalently written in terms of image samples instead of coefficients, hence reducing computations in the corresponding iterations (13) and (14).

For our implementation, we have simplified (13) by taking $a_t = b_t \equiv 0$ and $\beta_t \equiv 1$. As the PSF h in our experiments is low-pass normalized to a unit sum, $\|\mathrm{H}\|_2^2 = 1$. Ψ was the ℓ_1-norm, leading to soft-thresholding. Furthermore, in order to accelerate the computation of prox_{f_2} in (13), the Douglas-Rachford sub-iteration (10) was only run once (i.e. $N_{\mathrm{DR}} = 1$) starting with $\gamma^0 = \alpha$. One can check that this leads to the "natural" formula[3]:

$$\mathrm{prox}_{f_2}(\alpha) = \mathcal{P}_{\mathcal{C}'} \circ \mathrm{prox}_{\frac{\lambda}{2}\Psi}(\alpha).$$

In our experimental studies, the GCV-based selection of λ was run using the forward-backward algorithm (13) which has a lower computational burden than (14) (see above table for computational complexities). Once λ was objectively chosen by the GCV procedure, the deconvolution algorithm was applied using (14) to exempt the used from the choice of the relaxation parameter μ.

V. Results

A. Simulated data

The performance of our approach has been assessed on several test images: a 128×128 neuron phantom [34], a 370×370 confocal microscopy image of micro-vessel cells [35], the Cameraman (256×256), a 512×512 simulated astronomical image of the Hubble Space Telescope Wide Field Camera of a distant cluster of galaxies [3]. Our algorithm was compared to RL with total variation regularization (RL-TV [7]), RL with multi-resolution support wavelet regularization (RL-MRS [9]), fast translation invariant tree-pruning reconstruction combined with an EM algorithm (FTITPR [36]) and the naive proximal method that would treat the noise as if it were Gaussian (NaiveGauss [12]). For all results presented, each algorithm was run with $N_{\mathrm{FB}} = 200$ iterations, enough to reach

[3] γ^0 needs also to be in $\mathcal{C}'$.

convergence. For all results below, λ was selected using the GCV criterion for our algorithm. For fair comparison to [12], λ was also chosen by adapting our GCV formula to the Gaussian noise.

Fig.2(a), depicts a phantom of a neuron with a mushroom-shaped spine. The maximum intensity is 30. Its blurred (using a 7×7 moving average) and blurred+noisy versions are in (b) and (c). With this neuron, and for NaiveGauss and our approach, the dictionary Φ contained the curvelet tight frame [24]. The deconvolution results are shown in Fig.2(d)-(h). As expected at this intensity level, the worst result is given by the NaiveGauss algorithm, as it does not fit the noise model at this intensity regime. It turns out that NaiveGauss under-regularizes the estimate and the Poisson signal-dependent noise is not under control. This behavior of NaiveGauss, which was predictable at this intensity level, will be observed on all tested images. RL-TV does a good job at deconvolution but the background is dominated by artifacts, and the restored neuron has staircase-like artifacts typical of TV regularization. Our approach provides a visually pleasant deconvolution result on this example. It efficiently restores the spine, although the background is not fully cleaned. RL-MRS also exhibits good deconvolution results. On this image, FTITPR provides a well denoised estimate but with almost no deconvolution.

These qualitative visual results are confirmed by quantitative measures of the quality of deconvolution, where we used both the MAE (adapted to Poisson noise), and the traditional MSE criterion. At each intensity value, 10 noisy and blurred replications were generated and and the MAE was computed for each deconvolution algorithm. The average MAE over the 10 replications are given in Fig. 6 (similar results were obtained for the MSE, not shown here). In general, our algorithm performs very well especially at medium intensity regimes, whereas the NaiveGauss gives the worst MAE measure. RL-MRS is effective at low and medium intensity levels. RL-TV outperforms all algorithms at high intensity, but its MAE remains very comparable to ours.

The same experiment as above was carried out with the confocal microscopy cell image; see Fig. 3. In this experiment, the PSF was a 7×7 moving average. For the NaiveGauss and our approach, the dictionary Φ contained the translation-invariant discrete wavelet transform (TI-DWT). NaiveGauss deconvolution result is spoiled by artifacts. RL-TV produces a good restoration of small isolated details but with a dominating staircase-like artifacts. FTITPR and RL-MRS yield a somewhat oversmooth estimate, whereas our approach provides a sharper deconvolution result. This visual inspection is in agreement with the MAE measures of Fig. 6. In particular, one may notice that the performance of our approach compared to the other methods on this cell image is roughly the same as on the previous neuron image.

Fig.4(a) depicts the result of the experiment on the Cameraman with maximum intensity of 30. The PSF was the same as above. Again, the dictionary contained the TI-DWT frame. One may notice that the degradation in Fig.4(c) is quite severe. Our algorithm provides the most visually pleasing result with a good balance between regularization and deconvolution, although some artifacts are persisting. RL-MRS manages to deconvolve the image with more artifacts than our approach, and suffers from a loss of photometry. Again, FTITPR gives an oversmooth estimate with many missing details. Both RL-TV and NaiveGauss yield comparable results with many artifacts. This visual impression is in agreement with the MAE values in Fig. 6.

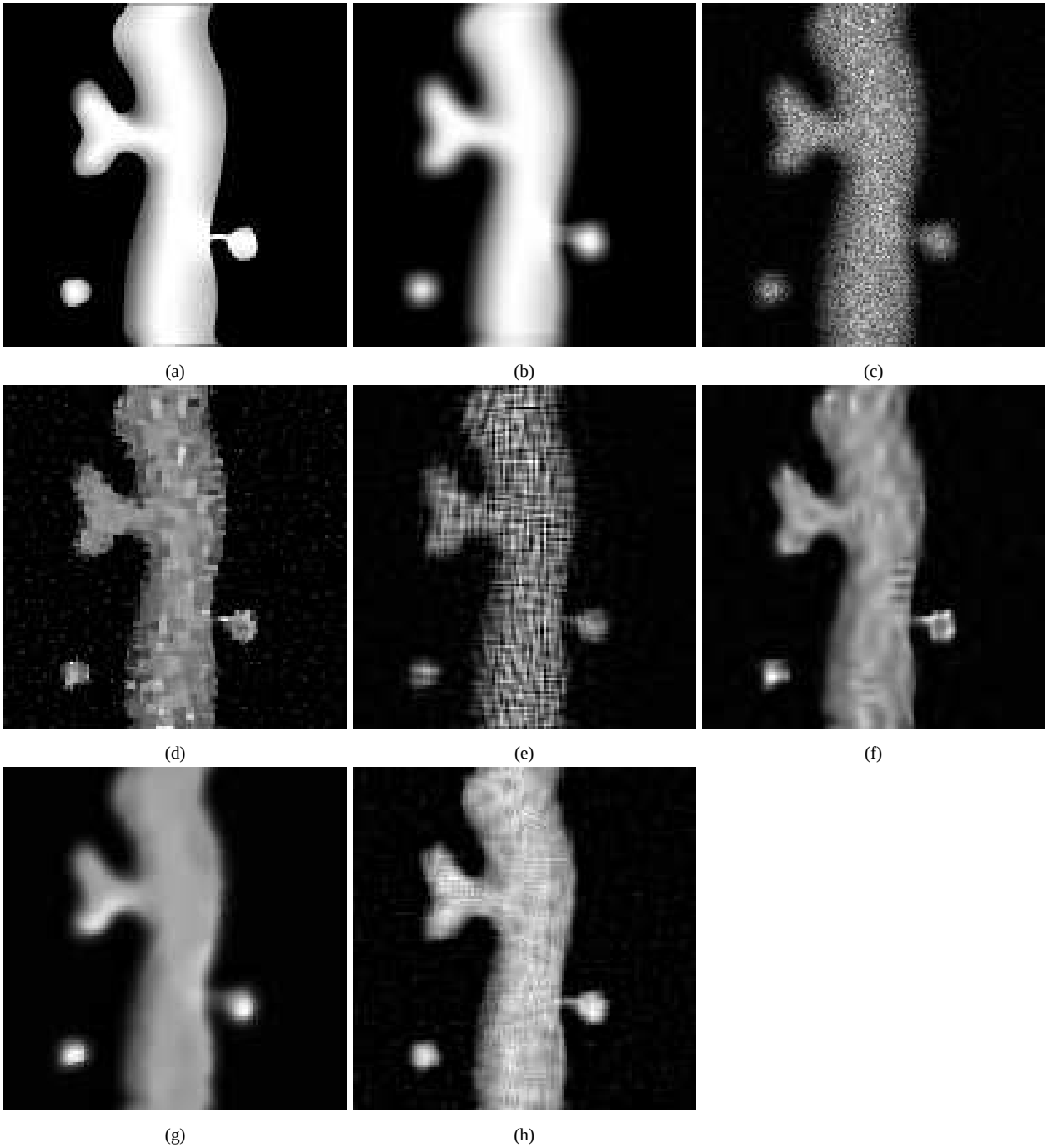

Figure 2. Deconvolution of a simulated neuron (Intensity $\leqslant 30$). (a) Original, (b) Blurred, (c) Blurred&noisy, (d) RL-TV [7], (e) NaiveGauss [12], (f) RL-MRS [3], (g) FTITPR [36], (h) Our Algorithm.

To assess the computational cost of the compared algorithms, Tab. I summarizes the execution times on the Cameraman image with an Intel PC Core 2 Duo 2GHz, 2Gb RAM. Except RL-MRS which is written in C++, all other algorithms were implemented in MATLAB.

The same experimental protocol was applied to a simulated Hubble Space Telescope wide field camera image of a distant cluster of galaxies portrayed in Fig.5(a). We used the Hubble Space Telescope PSF as given in [3]. For NaiveGauss and our approach, the dictionary contained the TI-DWT frame. For this image, the RL-MRS is clearly

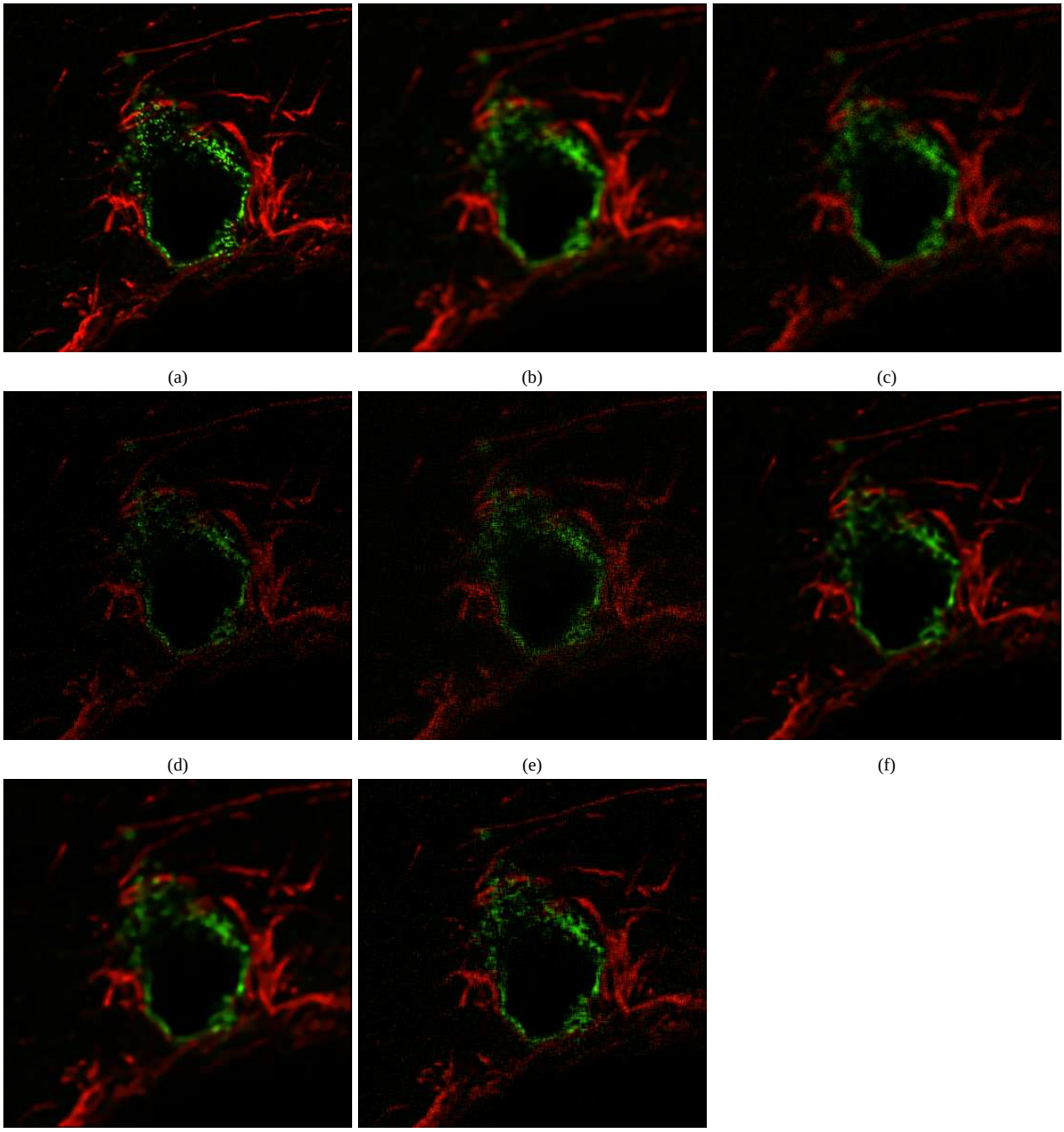

Figure 3. Deconvolution of a microscopy cell image (Intensity $\leqslant$ 30). (a) Original, (b) Blurred, (c) Blurred&noisy, (d) RL-TV [7], (e) NaiveGauss [12], (f) RL-MRS [3], (g) FTITPR [36] (h) Our Algorithm.

the best as it was exactly designed to handle Poisson noise for such images. Most faint structures are recovered by RL-MRS and large bright objects are well deconvolved. Our approach also yields a good deconvolution result and preserves most faint objects that are hardly visible on the degraded image. But the background is less clean than the one of RL-MRS. NaiveGauss fails to control the noise yielding an estimate dominated by artifacts. FTITPR manages to properly recover most significant structures with a very clean background, but many faint objects are lost. RL-TV gives a deconvolution result comparable to ours on the brightest objects, but the background is

Figure 4. Deconvolution of the cameraman (Intensity $\leqslant 30$). (a) Original, (b) Blurred, (c) Blurred&noisy, (d) RL-TV [7], (e) NaiveGauss [12], (f) RL-MRS [3], (g) FTITPR [36], (h) Our Algorithm.

dominated by spurious faint structures.

B. Real data

Finally, we applied our algorithm on a real 512×512 confocal microscopy image of neurons. Fig. 7(a) depicts the observed image[4] using the GFP fluorescent protein. The optical PSF of the fluorescence microscope was modeled

[4]Courtesy of the GIP Cycéron, Caen France.

Method	Time (in s)
Our method	88
NaiveGauss	71
RL-MRS	99.5
RL-TV	15.5

Table I

EXECUTION TIMES FOR THE SIMULATED 256×256 CAMERAMAN IMAGE USING THE TI-DWT ($N_{\mathrm{FB}} = 200$).

using the gaussian approximation described in [37]. Fig. 7(b) shows the restored image using our algorithm with the wavelet transform. The images are shown in log-scale for better visual rendering. We can notice that the background has been cleaned and some structures have reappeared. The spines are well restored and part of the dendritic tree is reconstructed. However, some information can be lost (see tiny holes). We suspect that this result may be improved using a more accurate PSF model.

VI. CONCLUSION

In this paper, a novel sparsity-based fast iterative thresholding deconvolution algorithm that takes account of the presence of Poisson noise was presented. The Poisson noise was handled properly. A careful theoretical study of the optimization problem, and characterization of the iterative algorithm were provided. The choice of the regularization parameter was also attacked using a GCV-based procedure. Several experimental tests have shown the capabilities of our approach, which compares favorably with some state-of-the-art algorithms. Encouraging preliminary results were also obtained on real confocal microscopy images.

The present work may be extended along several lines. For example, it is worth noting that our approach generalizes straightforwardly to any non-linearity in (1) other than the square-root, provided that the corresponding data fidelity term as in (4) has a Lipschitz-continuous gradient. On the applicative side, the extension to 3D to handle confocal microscopy volumes is under investigation. Extension to multi-valued images is also an important aspect that will be the focus of future research.

REFERENCES

[1] P. Sarder and A. Nehorai, "Deconvolution Method for 3-D Fluorescence Microscopy Images," *IEEE Sig. Pro. Mag.*, vol. 23, pp. 32–45, 2006.

[2] J. Pawley, *Handbook of Confocal Microscopy*. Plenum Press, 2005.

[3] J.-L. Starck and F. Murtagh, *Astronomical Image and Data Analysis*. Springer, 2006.

[4] H. C. Andrews and B. R. Hunt, *Digital Image Restoration*. Prentice-Hall, 1977.

[5] P. Jansson, *Image Recovery: Theory and Application*. New York: Academic Press, 1987.

[6] ——, *Deconvolution of Images and Spectra*. New York: Academic Press, 1997.

[7] N. Dey, L. Blanc-Fraud, C. Zimmer, Z. Kam, J.-C. Olivo-Marin, and J. Zerubia., "A deconvolution method for confocal microscopy with total variation regularization," in *IEEE ISBI*, 2004.

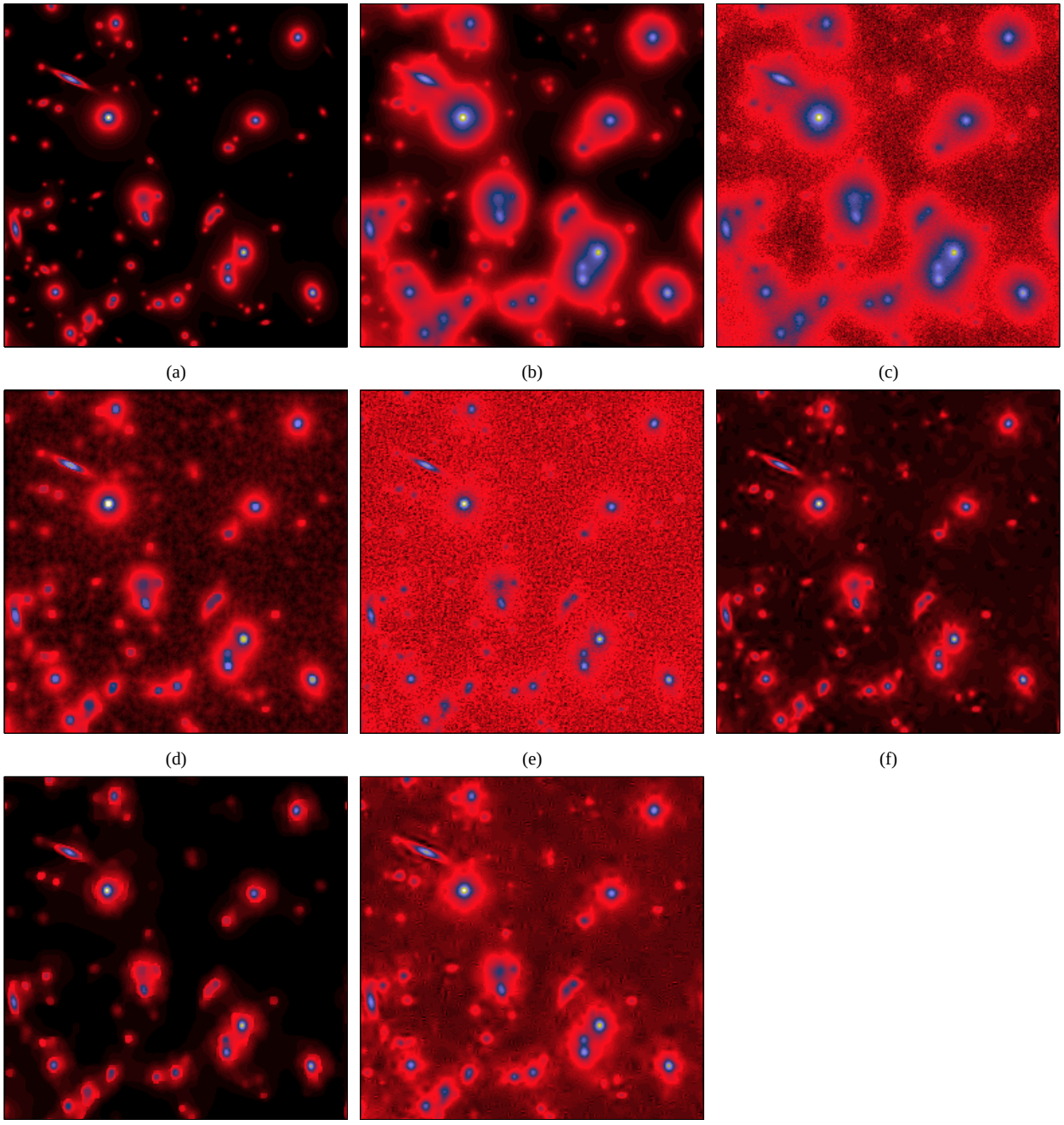

Figure 5. Deconvolution of the simulated sky. (a) Original, (b) Blurred, (c) Blurred&noisy, (d) RL-TV [7], (e) NaiveGauss [12], (f) RL-MRS [3], (g) FTITPR [36], (h) Our Algorithm.

[8] J.-L. Starck and F. Murtagh, “Image restoration with noise suppression using the wavelet transform,” *Astronomy and Astrophysics*, vol. 288, pp. 343–348, 1994.

[9] J.-L. Starck, A. Bijaoui, and F. Murtagh, “Multiresolution support applied to image filtering and deconvolution,” *CVGIP: Graphical Models and Image Processing*, vol. 57, pp. 420–431, 1995.

[10] G. Jammal and A. Bijaoui, “Dequant: a flexible multiresolution restoration framework,” *SP*, vol. 84, pp. 1049–1069, 2004.

[11] J. B. de Monvel et al, “Image Restoration for Confocal Microscopy: Improving the Limits of Deconvolution, with Application of the Visualization of the Mammalian Hearing Organ,” *Biophysical Journal*, vol. 80, pp. 2455–2470, 2001.

[12] C. Vonesch and M. Unser, “A fast iterative thresholding algorithm for wavelet-regularized deconvolution,” *IEEE ISBI*, 2007.

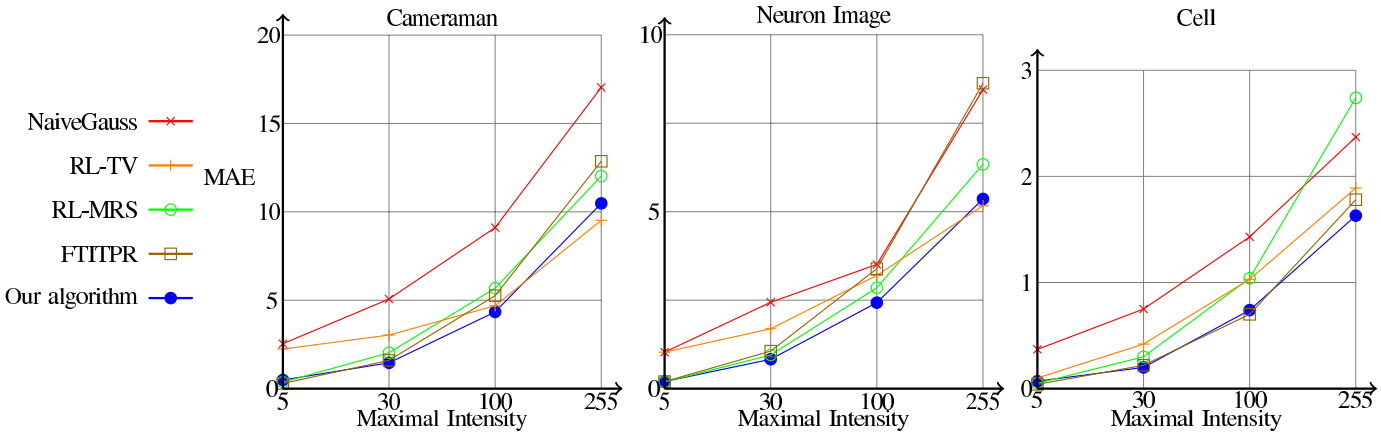

Figure 6. Average MAE of all algorithms as a function of the intensity level.

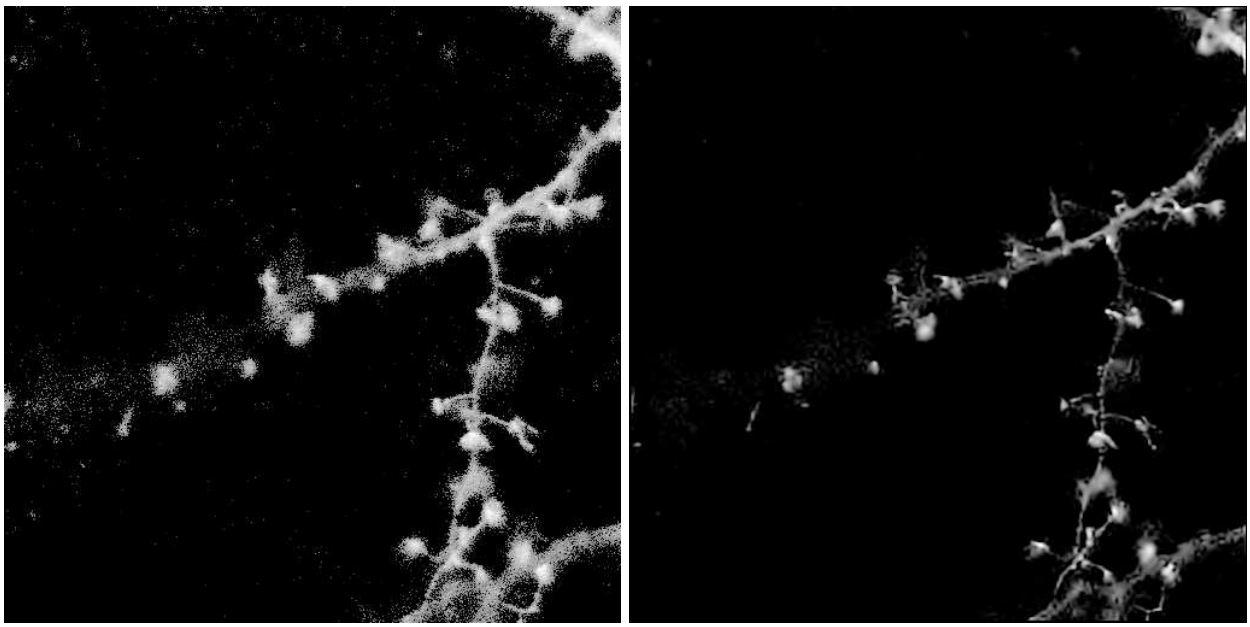

(a) (b)

Figure 7. Deconvolution of a real neuron. (a) Original noisy, (b) Restored with our algorithm

[13] I. Daubechies, M. Defrise, and C. D. Mol, "An iterative thresholding algorithm for linear inverse problems with a sparsity constraints," *CPAM*, vol. 112, pp. 1413–1541, 2004.

[14] M. Figueiredo and R. Nowak, "An em algorithm for wavelet-based image restoration," *IEEE Transactions on Image Processing*, vol. 12, pp. 906–916, 2003.

[15] P. L. Combettes and V. R. Wajs, "Signal recovery by proximal forward-backward splitting," *SIAM MMS*, vol. 4, no. 4, pp. 1168–1200, 2005.

[16] G. Teschke, "Multi-frame representations in linear inverse problems with mixed multi-constraints," *ACHA*, vol. 22, no. 1, pp. 43–60, 2007.

[17] C. Chaux, P. L. Combettes, J.-C. Pesquet, and V. R. Wajs, "A variational formulation for frame-based inverse problems," *Inv. Prob.*, vol. 23, pp. 1495–1518, 2007.

[18] M. J. Fadili and J.-L. Starck, "Sparse representation-based image deconvolution by iterative thresholding," in *ADA IV*. France: Elsevier, 2006.

[19] J.-L. Starck, M. Nguyen, and F. Murtagh, "Wavelets and curvelets for image deconvolution: a combined approach," *Signal Processing*,

vol. 83, pp. 2279–2283, 2003.

[20] C. Chaux, L. Blanc-Féraud, and J. Zerubia, "Wavelet-based restoration methods: application to 3d confocal microscopy images," in *SPIE Wavelets XII*, 2007.

[21] F. J. Anscombe, "The Transformation of Poisson, Binomial and Negative-Binomial Data," *Biometrika*, vol. 35, pp. 246–254, 1948.

[22] S. G. Mallat, *A Wavelet Tour of Signal Processing*, 2nd ed. Academic Press, 1998.

[23] E. J. Candès and D. L. Donoho, "Curvelets – a surprisingly effective nonadaptive representation for objects with edges," in *Curve and Surface Fitting: Saint-Malo 1999*, A. Cohen, C. Rabut, and L. Schumaker, Eds. Nashville, TN: Vanderbilt University Press, 1999.

[24] E. Candès, L. Demanet, D. Donoho, and L. Ying, "Fast discrete curvelet transforms," *SIAM Multiscale Model. Simul.*, vol. 5, pp. 861–899, 2005.

[25] L. Demanet and L. Ying, "Wave atoms and sparsity of oscillatory patterns," *ACHA*, vol. 23, no. 3, pp. 368–387, 2007.

[26] J.-J. Moreau, "Fonctions convexes duales et points proximaux dans un espace hilbertien," *CRAS Sér. A Math.*, vol. 255, pp. 2897–2899, 1962.

[27] J. Eckstein and D. P. Bertsekas, "On the Douglas-Rachford splitting method and the proximal point algorithm for maximal monotone operators," *Math. Programming*, vol. 55, pp. 293–318, 1992.

[28] P.-L. Lions and B. Mercier, "Splitting algorithms for the sum of two nonlinear operators," *SIAM J. Numer. Anal.*, vol. 16, pp. 964–979, 1979.

[29] P. L. Combettes, "Solving monotone inclusions via compositions of nonexpansive averaged operators," *Optimization*, vol. 53, pp. 475–504, 2004.

[30] M. Fadili, J.-L. Starck, and F. Murtagh, "Inpainting and zooming using sparse representations," *The Computer Journal*, 2006, in press.

[31] P. L. Combettes and J.-C. Pesquet, "Proximal thresholding algorithm for minimization over orthonormal bases," *SIAM Journal on Optimization*, vol. 18, no. 4, pp. 1351–1376, November 2007.

[32] P. Tseng, "A modified forward-backward splitting method for maximal monotone mappings," *SIAM J. Control & Optim.*, vol. 38, pp. 431–446, 2000.

[33] G. H. Golub, M. Heath, and G. Wahba, "Generalized cross-validation as a method for choosing a good ridge parameter," *Technometrics*, vol. 21, no. 2, pp. 215–223, 1979.

[34] [Online]. Available: RebeccaWilletthomepagehttp://www.ee.duke.edu/~willett/

[35] [Online]. Available: ImageJwebsitehttp://rsb.info.nih.gov/ij/

[36] R. Willett and R. Nowak, "Fast multiresolution photon-limited image reconstruction," *IEEE ISBI*, 2004.

[37] B. Zhang, J. Zerubia, and J.-C. Olivo-Marin, "Gaussian approximations of fluorescence microscope PSF models," *Applied Optics*, vol. 46, no. 10, pp. 1819–1829, 2007.

[38] P. L. Combettes and J.-. Pesquet, "A Douglas-Rachford splittting approach to nonsmooth convex variational signal recovery," *IEEE Journal on STSP*, 2007, to appear.

[39] L. A. Karlovitz, "Construction of nearest points in the l_p, p even and l_1 norms," *Journal of Approximation Theory*, vol. 3, pp. 123–127, 1970.

[40] I. F. Gorodnitsky and B. D. Rao, "Sparse signal reconstruction from limited data using FOCUSS: A re-weighted minimum norm algorithm," *ITSP*, vol. 45, no. 3, pp. 600–616, 1997.

APPENDIX

A. Proof of Proposition 1

Proof:

(i) f_1 is obviously convex, as Φ and H are bounded linear operators and f is convex.

(ii) The computation of the gradient of f_1 is straightforward.

(iii) For any $\alpha, \alpha' \in \mathcal{H}$, we have,

$$\left\|\nabla f_1(\alpha) - \nabla f_1(\alpha')\right\| \leqslant \|\Phi\|_2 \|\mathrm{H}\|_2 \left\|\nabla F \circ \mathrm{H} \circ \Phi(\alpha) - \nabla F \circ \mathrm{H} \circ \Phi(\alpha')\right\|. \tag{18}$$

The function $-\frac{z_i}{\sqrt{\eta_i+3/8}} + 2$ is one-to-one increasing on $(0, +\infty)$ with derivative uniformly bounded above by $\frac{z_i}{2}(8/3)^{3/2}$. Thus,

$$\begin{aligned}\left\|\nabla F \circ \mathrm{H} \circ \Phi(\alpha) - \nabla F \circ \mathrm{H} \circ \Phi(\alpha')\right\| &\leqslant \left(\frac{8}{3}\right)^{\frac{3}{2}} \frac{\|z\|_\infty}{2} \left\|\mathrm{H} \circ \Phi(\alpha) - \mathrm{H} \circ \Phi(\alpha')\right\| \\ &\leqslant \left(\frac{8}{3}\right)^{\frac{3}{2}} \frac{\|z\|_\infty}{2} \|\Phi\|_2 \|\mathrm{H}\|_2 \left\|\alpha - \alpha'\right\| . \end{aligned} \tag{19}$$

Using the fact that $\|\Phi\|_2^2 = \left\|\Phi\Phi^{\mathrm{T}}\right\|_2 = c$ for a tight frame, and z is bounded since $y \in \ell_\infty$ by assumption, we conclude that ∇f_1 is Lipschitz-continuous with the constant given in (8).

■

B. Proof of Proposition 2

Proof: The existence is obvious because J is coercive. If Φ is an orthobasis and $\ker(H) = \emptyset$ then f_1 is strictly convex and so is J leading to a strict minimum. Similarly, if ψ is strictly convex, so is f_2, hence J. ■

C. Proof of Lemma 1

Proof:

1) Let $g : \gamma \mapsto \frac{1}{2}\|\alpha - \gamma\|^2 + \lambda\Psi(\gamma)$. From Definition 1, $\mathrm{prox}_{\lambda\Psi}(\alpha)$ is the unique minimizer of g, whereas $\mathrm{prox}_{f_2}(\alpha)$ is the unique minimizer of $g + \imath_{\mathcal{C}'}$. If $\alpha \in \mathcal{C}'$, then $\mathrm{prox}_{f_2}(\alpha)$ is also the unique minimizer of g as obviously $\imath_{\mathcal{C}'}(\alpha) = 0$ in this case. That is, $\mathrm{prox}_{f_2}(\alpha) = \mathrm{prox}_{\lambda\Psi}(\alpha)$.
2) Let's now turn to the general case. We have to find the unique solution to the following minimization problem:

$$\mathrm{prox}_{f_2}(\alpha) = \arg\min_{\gamma} \; g(\gamma) + \imath_{\mathcal{C}} \circ \Phi(\gamma) = \arg\min_{\gamma \in \mathcal{C}'} \; g(\gamma).$$

As both $\imath_{\mathcal{C}}$ and $g \in \Gamma_0(\mathcal{H})$ but non-differentiable, we use the Douglas-Rachford splitting method [27], [29]. This iteration is given by:

$$\gamma^{t+1} = \gamma^t + \nu_t \left(\mathrm{rprox}_{\lambda\Psi + \frac{1}{2}\|.-\alpha\|^2} \circ \mathrm{rprox}_{\imath_{\mathcal{C}'}} - \mathrm{I}\right)(\gamma^t). \tag{20}$$

where the sequence ν_t satisfies the condition of the lemma. From [29, Corollary 5.2], and by strict convexity, we deduce that the sequence of iterates γ^t converges weakly to a unique point γ, and $\mathcal{P}_{\mathcal{C}'}(\gamma)$ is the unique proximity point $\mathrm{prox}_{f_2}(\alpha)$.

It remains now to explicitly express $\mathrm{prox}_{\lambda\Psi + \frac{1}{2}\|.-\alpha\|^2}$ and $\mathrm{prox}_{\imath_{\mathcal{C}'}}$. $\mathrm{prox}_{\lambda\Psi + \frac{1}{2}\|.-\alpha\|^2}$ is the proximity operator of a quadratic perturbation of $\lambda\Psi$, which is related to $\mathrm{prox}_{\lambda\Psi}$ by:

$$\mathrm{prox}_{\lambda\Psi + \frac{1}{2}\|.-\alpha\|^2}(.) = \mathrm{prox}_{\frac{\lambda}{2}\Psi}\left(\frac{\alpha + .}{2}\right). \tag{21}$$

See [15, Lemma 2.6].

Using [38, Proposition 11], we have

$$\begin{aligned} \mathrm{prox}_{\iota_C \circ \Phi} &= \mathrm{I} + c^{-1}\Phi^{\mathrm{T}} \circ (\mathcal{P}_{\mathcal{C}} - \mathrm{I}) \circ \Phi \\ &= c^{-1}\Phi^{\mathrm{T}} \circ \mathcal{P}_{\mathcal{C}} \circ \Phi + (\mathrm{I} - c^{-1}\Phi^{\mathrm{T}}\Phi). \end{aligned} \tag{22}$$

This completes the proof. ■

D. Proof of Theorem 1

Proof: The most general result on the convergence of the Forward-Backward algorithm is is due to [15, Theorem 3.4]. Hence, combining this theorem with Lemma 1, Lemma 2 and Proposition 1, the result follows. ■

E. Derivation of the approximate GCV formula

The following developments rely on two ingredients : (i) the degradation equation (1) is linearized, and (ii) the ℓ_1-norm is rewritten in the form of a re-weighted ℓ_2-norm. The latter trick is in the same vein as what is used by the IRLS and FOCUSS algorithms [39], [40].

Let $d = \frac{3}{8}$ and denote $\mathrm{A} = \mathrm{H}\Phi$. Recall that z denotes our observation $z = 2\sqrt{\mathrm{H}\Phi\alpha + d} + \varepsilon,\ \varepsilon \sim \mathcal{N}(0,1)$.

We first linearize (1) by means of the Taylor formula to the first order:

$$z = 2d^{1/2} + d^{-1/2}\mathrm{A}\alpha + r(\alpha) + \varepsilon\ , \tag{23}$$

where the rest satisfies $\lim_{\alpha \to 0} \frac{r(\alpha)}{\|\alpha\|} = 0$. This rest will be neglected hereafter.

Let $u = \sqrt{2}z - 2d = \mathrm{H}\Phi\alpha + \varepsilon'$, where $\varepsilon' \sim \mathcal{N}(0, d)$. From the modified degradation problem, we are now able to formulate the following penalized least-squares problem:

$$\min_{\alpha} \tfrac{1}{2} \left\| u - \mathrm{A}\alpha \right\|^2 + \tau \left\| \mathrm{W}^{-1}\alpha \right\|^2, \tag{24}$$

where $\tau = \lambda d$, and W^{-1} is a diagonal weight matrix with $1/\sqrt{|\alpha_i|}$ as its main diagonal entries (assume that for $\alpha_i = 0$ the weight is chosen to be some finite high value in order to avoid infinity). Formed as such, we can use simple least-squares to solve this problem with W assumed to be fixed. It can be shown that,

$$\tilde{\alpha} \ = \ \left(\mathrm{A}^{\mathrm{T}}\mathrm{A} + \tau\mathrm{W}^{-2}\right)^{-1} \mathrm{A}^{\mathrm{T}} u = \mathrm{W}^2\mathrm{A}^{\mathrm{T}} \left(\mathrm{A}\mathrm{W}^2\mathrm{A}^{\mathrm{T}} + \tau\right)^{-1} u\ . \tag{25}$$

Let $\tilde{y} = \mathrm{A}\tilde{\alpha} = \mathrm{B}u$, where $\mathrm{B} = \mathrm{A}\mathrm{W}^2\mathrm{A}^{\mathrm{T}}(\mathrm{A}\mathrm{W}^2\mathrm{A}^{\mathrm{T}} + \tau)^{-1}$ is the so-called hat matrix or the derivative influence matrix [33]. Thus, the GCV is given by:

$$\mathrm{GCV}(\lambda) = \frac{\left\| z - 2\sqrt{\mathrm{A}\alpha^* + d} \right\|^2}{df^2} \approx \frac{\left\| z - 2\sqrt{\mathrm{A}\alpha^* + d} \right\|^2}{\mathrm{tr}\ [\mathrm{I} - \mathrm{B}]^2}, \tag{26}$$

where α^* is the estimate which has been computed using our restoration algorithm, and df is the effective number of degrees of freedom defined through the influence matrix. In (26), the $\approx$ symbol originates from the above simplifying assumptions. However, computing df necessitates a matrix inversion that involves the large matrices

H and Φ. These cannot be constructed explicitly. Consequently, the expression of $df = \mathrm{tr}\ [\mathrm{I} - \mathrm{B}]$ is not easy to compute in practice. We then propose to approximate the weight matrix by a diagonal one such that $\mathrm{W}^2 \approx \|\alpha^*\|_\infty \mathrm{I}$. In such a case,

$$\begin{aligned}
\mathrm{B} &= \|\alpha^*\|_\infty \mathrm{A}\mathrm{A}^{\mathrm{T}} \left(\|\alpha^*\|_\infty \mathrm{A}\mathrm{A}^{\mathrm{T}} + \tau\right)^{-1} \\
&= \|\alpha^*\|_\infty c\mathrm{H}\mathrm{H}^* \left(\|\alpha^*\|_\infty c\mathrm{H}\mathrm{H}^* + \tau\right)^{-1} \\
&= \|\alpha^*\|_\infty c\mathrm{U}\,\mathrm{diag}\left(\left(|\hat{h}_i|^2\right)_i\right)\left(\|\alpha^*\|_\infty c\,\mathrm{diag}\left(\left(|\hat{h}_i|^2\right)_i\right) + \tau\right)^{-1}\mathrm{U}^*,
\end{aligned}$$

where we used the fact that the convolution operator H is diagonalized in the discrete Fourier basis U, i.e. $\mathrm{H} = \mathrm{U}\,\mathrm{diag}\left((\hat{h}_i)_{1\leqslant i\leqslant n}\right)\mathrm{U}^*$, and $\Phi\Phi^T = c\mathrm{I}$ when Φ is a tight frame. df has then a closed-form expression given by:

$$df \approx \sum_i \left(\frac{\lambda}{\lambda + \frac{8c}{3}\|\alpha^*\|_\infty |\hat{h}_i|^2}\right) . \tag{27}$$